J. Fluid Mech. (1981), *vol.* 112, *pp.* 265-282
Printed in Great Britain

Approximate and exact numerical computation of supersonic flow over an airfoil

By TIMOTHY S. LEWIS AND LAWRENCE SIROVICH

Division of Applied Mathematics,
Brown University, Providence, Rhode Island 02912

(Received 24 January 1980)

An approximate solution is developed for two-dimensional, steady, inviscid supersonic flow over an airfoil. This approximation produces accurate results for a wide range of Mach numbers and airfoil thicknesses. It is used as the starting point for a rapidly convergent iterative numerical solution of the exact equations. A co-ordinate system consisting of the principal characteristics and streamlines is employed. Examples computed for a symmetric airfoil reveal several interesting features in the tail shock and the flow behind the airfoil.

1. Introduction

In this paper we consider the computation of inviscid supersonic flow over a two-dimensional airfoil. While the final step in our investigation is numerical, we attempt to incorporate as much as possible our analytical and physical knowledge of such flows. The approach is well suited both for numerical integration and for the interpretation of the resulting flow phenomena. A preliminary version of this approach for the case of one-dimensional unsteady flow has already been reported (Sirovich & Chong 1980; Chong & Sirovich 1980). In the present investigation several new or little-known effects concerning the tail shock and flow behind a two-dimensional airfoil emerge. These are discussed in § 6.

There are two main nonlinear approximations for this problem. Small-amplitude theory gives solutions valid provided the airfoil thickness is not too great and the Mach number is not too high. Under these conditions the leading shock wave is fairly weak and the solution is approximately given by a simple wave involving only the characteristics emanating from the airfoil (Friedrichs 1948; Lighthill 1960). Variations in the entropy and in the Riemann invariant which is carried along the down-running characteristics are only of third order in the shock strength, so the resulting approximation is valid to second order. A correction in the tail shock region is necessary to obtain a second-order solution there (Caughey 1969).

The second type of approximation, shock expansion theory, originated by Epstein (1931), employs the fact that even for flows with strong shocks, for which the assumptions of small perturbation theory do not hold, the effect of the down-running characteristics remains small. This leads to an analytic solution at the airfoil, which has been generalized by several authors (Eggers, Syvertson & Kraus 1953; Meyer 1957) to provide approximate solutions for the entire flow field. In another approach, Jones

(1963) has derived by a perturbation method an approximate solution between simple wave theory and generalized shock expansion theory.

In § 4 we derive an approximate solution which is closely related to these, but which applies its assumptions more consistently and is somewhat more accurate. This approximation includes both shock expansion theory and the second-order theories of Friedrichs and Caughey. The derivation and the numerical computation of the solution are facilitated by the use of the principal characteristics and the streamlines as co-ordinates (§ 3). Adamson (1968) has used a similar co-ordinate system in another context. For a problem in which the down-running characteristics are also important (e.g. flow in a nozzle), this approach is less appropriate.

The approximate solution is used as the starting point for an iterative numerical computation of the exact solution (§ 5). The high accuracy of the approximation leads to the exact solution after only a few iterations. This procedure is different from most numerical methods for hyperbolic problems. Typical methods apply one of a variety of differencing schemes (for a comparison of several such schemes see Taylor, Ndefo & Masson 1972) to the equations in their standard form and compute the solution by 'marching' along in the downstream direction. One disadvantage of these methods is that at low Mach numbers short step sizes are required for stability. The method of characteristics (Liepmann & Roshko 1957, cha. 12) can also be used for this problem, although it is considered in general to be somewhat unwieldy for machine computation. The BVLR method (Babenko *et al.* 1966; Holt 1977) is a finite-difference method which is partly based upon the method of characteristics. The transformation of co-ordinates employed here also results in a method which is closely related to the method of characteristics.

Special account must be taken of the appearance of shock waves in this type of problem. In finite-difference methods this can be done through shock-capturing difference schemes, or through explicit shock fitting (e.g. Salas 1976). In the present method the shock waves can be naturally incorporated in the new co-ordinate system as fixed boundaries of the flow field.

2. Formulation of problem

We consider uniform flow of Mach number $M_0 > 1$ incident upon a two-dimensional airfoil (see figure 1). It is assumed that there are attached shocks at the leading and trailing edges, and that the flow remains supersonic everywhere. The flow fields above and below the airfoil can be computed independently, up to the appearance of the tail shocks. The tail shock and the flow behind it for the case of a symmetric airfoil are treated in appendix B.

The co-ordinates x and y are scaled by the airfoil length; the pressure p and the density ρ by their upstream values p_0 and ρ_0; the velocity $(u, v) = (q\cos\theta, q\sin\theta)$ and the speed of sound a by the upstream speed of sound a_0; and the entropy s, which is set to zero upstream, by the gas constant R. We consider a perfect gas with constant specific heats $c_v = R/(\gamma - 1)$ and $c_p = \gamma c_v$, for which the equation of state is

$$p = \rho^\gamma \exp\left[(\gamma - 1)\, s\right]$$

and the speed of sound is given by $a^2 = p/\rho$. The calculations here were done for $\gamma = 1{\cdot}4$. Modifications for the case of a gas with a general equation of state are outlined in appendix A.

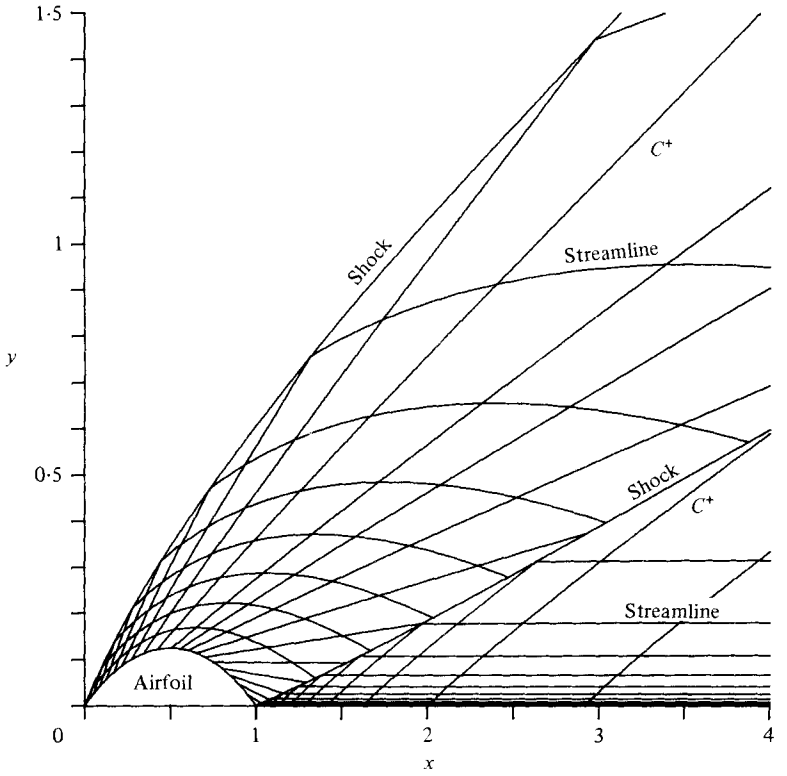

FIGURE 1. Supersonic flow over a symmetric 25 % thick circular arc airfoil at upstream Mach number $M_0 = 2{\cdot}5$.

The equations of inviscid two-dimensional steady flow are conveniently written with the entropy s, the flow angle θ, and the Mach angle $\mu = \sin^{-1}(1/M)$ (where $M = q/a$ is the local Mach number) as dependent variables. All other physical quantities can be obtained from these and Bernoulli's equation

$$a^2 + \frac{\gamma - 1}{2} q^2 = 1 + \frac{\gamma - 1}{2} M_0^2. \tag{1}$$

The equations of motion in characteristic form are (Meyer 1960, p. 273)

$$ds = 0 \quad \text{on streamlines} \quad \frac{dy}{dx} = \tan\theta; \tag{2}$$

$$d(\theta \pm P(\mu)) = \pm \frac{\sin 2\mu}{2\gamma} ds \quad \text{on } C^{\pm} \quad \frac{dy}{dx} = \tan(\theta \pm \mu); \tag{3}$$

where $P(\mu)$ is given by

$$P(\mu) = \lambda^{\frac{1}{2}} \tan^{-1}(\lambda^{\frac{1}{2}} \tan\mu) - \mu, \quad \lambda = (\gamma + 1)/(\gamma - 1).$$

The streamlines and the C^+ characteristics are shown in figure 1. The quantities $r^{\pm} = \theta \pm P(\mu)$ are called the Riemann invariants.

If the airfoil surface is specified as $y = f(x)$, the appropriate boundary condition there is

$$\tan\theta = f'(x) \quad \text{on} \quad y = f(x). \tag{4}$$

The jumps in θ, μ and s across a shock are governed by the Rankine–Hugoniot conditions (Liepmann & Roshko 1957, p. 85). All three quantities can be written as explicit functions of M_0, γ and the shock angle, η.

3. New co-ordinate system

As mentioned in the introduction, in a problem with weak shock waves deviations in s and r^- from their upstream values are third-order quantities. This is shown in figure 2, where Δs and Δr^- are plotted on a logarithmic scale against the deflection angle θ, for several Mach numbers. As $\theta \to 0$, the curves approach straight lines of slope 3. While Δs and Δr^- are both third-order quantities, for a given Mach number the jump in r^- is always significantly smaller than that in s. This suggests that for weak to moderate strength shock waves the flow field can be considered primarily an interaction between a simple wave and an entropy variation, with r^- playing only a small role.

This leads us to introduce a co-ordinate system (α, β) consisting of the streamlines, α = constant, and the principal (C^+) characteristics, β = constant. Taking α and β as the independent variables, x and y must satisfy

$$y_\beta = x_\beta \tan\theta, \quad y_\alpha = x_\alpha \tan(\theta+\mu). \tag{5}$$

The entropy equation (2) becomes

$$s_\beta = 0, \tag{6}$$

or $s = s(\alpha)$. Equations $(3+)$ and $(3-)$ become

$$(\theta + P(\mu))_\alpha = \frac{\sin 2\mu}{2\gamma} s'(\alpha) \tag{7}$$

and

$$\left(\frac{\partial}{\partial\alpha} + w\frac{\partial}{\partial\beta}\right)(\theta - P(\mu)) = -\frac{\sin 2\mu}{2\gamma} s'(\alpha), \tag{8}$$

where

$$w = -\frac{2}{1-\tan\theta\tan\mu}\left(\frac{x_\alpha}{x_\beta}\right). \tag{9}$$

Using (7), equation (8) can be simplified to

$$(\theta - P(\mu))_\beta = (1-\tan\theta\tan\mu)\frac{x_\beta}{x_\alpha}\theta_\alpha. \tag{10}$$

Equations (5)–(7) and (10) are five equations in five unknowns: θ, μ, s, x and y.

The boundary and shock conditions in the $\alpha\beta$ plane can be simplified by normalizing α and β appropriately. We let the airfoil surface be the streamline $\alpha = 0$, and normalize β by setting $\beta = x$ at $\alpha = 0$. The boundary condition (4) then becomes

$$x(0,\beta) = \beta, \quad y(0,\beta) = f(\beta), \quad \theta(0,\beta) = \tan^{-1}f'(\beta). \tag{11}$$

One convenient way of normalizing α is to take the front shock angle $\eta(\alpha)$ to be given by

$$\tan\eta(\alpha) = (1-\alpha)\tan\eta(0) + \alpha\tan\mu_0, \tag{12}$$

where $\eta(0)$ is known from solving the shock conditions at the leading edge, and μ_0 is the upstream Mach angle, which the shock approaches far away from the airfoil.

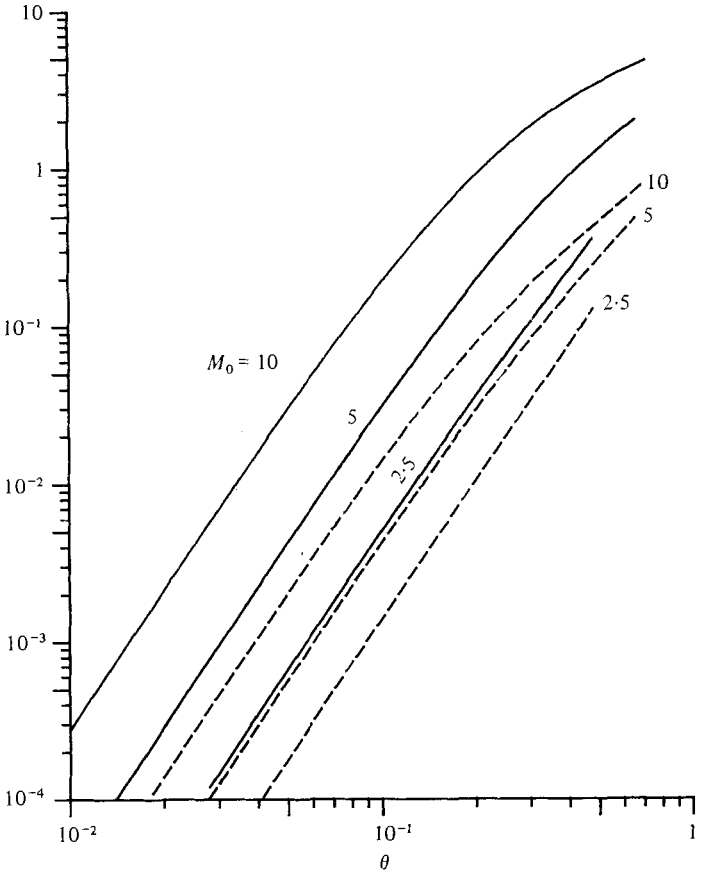

FIGURE 2. Jumps in entropy s and Riemann invariant r^- across a shock wave as functions of deflection angle θ, at various Mach numbers: ——, Δs; – – –, Δr^-.

Hence $\alpha = 1$ corresponds to $x, y \to \infty$. If η is not a strictly decreasing function, a different normalization must be used. The flow field in the upper half-plane is mapped into a finite region in the $\alpha\beta$ plane, as shown in figure 3. The principal characteristics become vertical lines, and the streamlines become horizontal lines. The front shock maps into some curve $\beta(\alpha)$, and the left- and right-hand sides of the tail shock into two separate curves $\beta_2(\alpha)$ and $\beta_3(\alpha)$. The discussion of the tail shock is left to appendix B. With the shock angle $\eta(\alpha)$ a given function, the shock conditions can be immediately solved for $\theta(\alpha, \beta(\alpha))$, $\mu(\alpha, \beta(\alpha))$, and $s(\alpha)$. The shock $\beta(\alpha)$ itself will in general depend on the rest of the solution, however.

It is possible to eliminate y from the equations by setting $y_{\alpha\beta} = y_{\beta\alpha}$ in (5). Using (10), this gives

$$0 = x_{\alpha\beta}/x_\alpha + (\mu + P(\mu))_\beta \cot\mu + (\theta+\mu)_\beta \tan(\theta+\mu), \tag{13}$$

which can be integrated to

$$x(\alpha,\beta) = x(0,\beta) + \int_0^\alpha A(\alpha)\, a^{-\lambda} \cos(\theta+\mu)\, d\alpha, \tag{14}$$

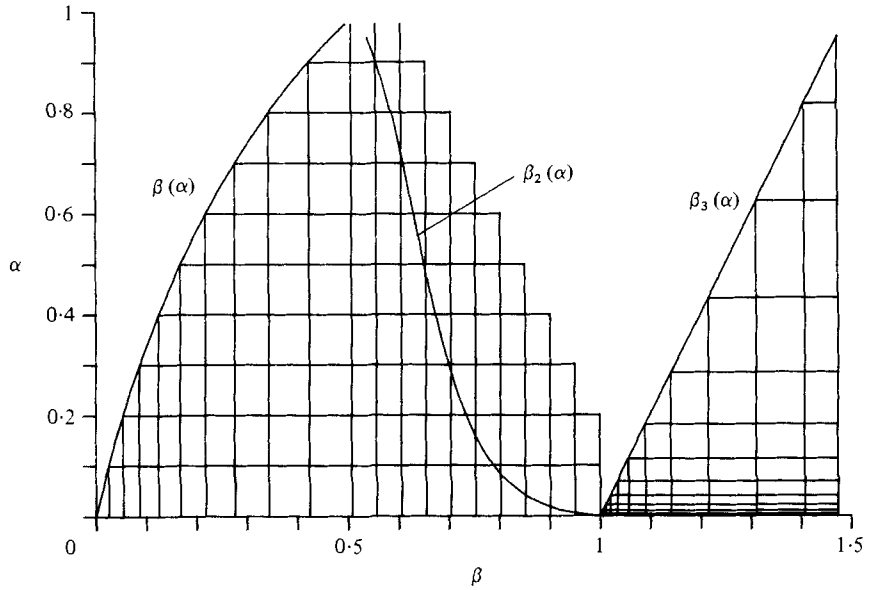

FIGURE 3. Flow field corresponding to figure 1 in $\alpha\beta$ plane. Streamlines map into horizontal lines, α = const., and C^+ characteristics into vertical lines, β = const. Front shock maps into $\beta(\alpha)$, and left and right sides of tail shock into $\beta_2(\alpha)$ and $\beta_3(\alpha)$, respectively.

where $A(\alpha)$ is an arbitrary function to be determined later, and we recall

$$\lambda = (\gamma+1)/(\gamma-1).$$

Similarly, from (5) we get

$$y(\alpha,\beta) = y(0,\beta) + \int_0^\alpha A(\alpha)\, a^{-\lambda} \sin(\theta+\mu)\, d\alpha. \tag{15}$$

At $\beta = \beta(\alpha)$ the condition

$$\tan\eta = \frac{dy}{dx} = \frac{x_\alpha + y_\beta \beta'(\alpha)}{y_\alpha + x_\beta \beta'(\alpha)} \tag{16}$$

must be satisfied. Elimination of y using (5) and substitution of (14) for x produces a linear integral equation for $A(\alpha)$:

$$A(\alpha)\, Q(\alpha,\beta(\alpha)) + b(\alpha)\left[1 + \int_0^\alpha A(\hat{\alpha})\, Q_\beta(\hat{\alpha},\beta(\alpha))\, d\hat{\alpha}\right] = 0, \tag{17}$$

where $Q = a^{-\lambda}\cos(\theta+\mu)$, and

$$b(\alpha) = \beta'(\alpha)\left.\frac{\tan\eta - \tan\theta}{\tan\eta - \tan(\theta+\mu)}\right|_{\beta=\beta(\alpha)}.$$

If the solution for θ, μ and s is known in the $\alpha\beta$ plane, this equation can be solved for $A(\alpha)$, and the transformation back to the physical plane computed with (14) and (15). In general, however, the solution in the $\alpha\beta$ plane depends on x, through (10).

Up to this point the equations in $\alpha\beta$ co-ordinates have been derived without approximation, and hence are equivalent to the original set (2) and (3).

4. Approximate solutions

If the third-order changes in s and r^- are neglected, that is, it is assumed that $s = 0$ and $r^- = -P(\mu_0)$ everywhere, the solution of (2) and (3) is a simple wave, in which all quantities are constant on the principal (C^+) characteristics, which in turn are straight lines:

$$\theta = \tan^{-1} f'(\beta), \quad \mu = P^{-1}(\theta + P(\mu_0)), \quad s = 0 \quad \text{on } C^+:$$
$$y = f(\beta) + (x - \beta)\tan(\theta + \mu).$$

This approximation is due to Friedrichs (1948). (Friedrichs further simplified the problem by neglecting terms of third and higher order throughout the calculation.)

Because simple wave theory takes s and r^- constant at their upstream values, it can be expected to be least accurate near the airfoil, where the shock is strongest and the deviation from upstream conditions is the greatest. An improved approximation in this region can be obtained using shock expansion theory, in which s and r^- are assumed to be constant at their values just behind the shock at the leading edge, say $s = s_0$ and $r^- = r_0^-$. This leads to a slightly modified version of the simple wave solution:

$$\theta = \tan^{-1} f'(\beta), \quad \mu = P^{-1}(\theta - r_0^-), \quad s = s_0.$$

This approximation produces a very accurate solution at the airfoil, even for flows with strong shocks, in which s and r^- are not at all constant globally. Hayes & Probstein (1966) explain that the down-running waves, which can be considered reflections of the outgoing simple wave by the bow shock, are fairly weak and are nearly cancelled by reflections from the entropy (or vorticity) layers. Mahony (1955) gives a similar explanation. The shock expansion solution rapidly loses accuracy as the distance from the airfoil increases. This is in contrast to simple wave theory, which is more accurate at infinity.

The only assumption in the shock expansion solution at the airfoil is that r^- is constant. Mahony & Skeat (1955) and Meyer (1957) have pointed out that, since any streamline is a potential airfoil, r^- should be approximately constant along each streamline, that is $r^- = r^-(\alpha)$. In the literature this assumption has been employed in various ways. If $r^- = r^-(\alpha)$, then by (10) $\theta = \theta(\beta)$, i.e. θ is constant on C^+ characteristics. This in turn implies that the pressure is constant on C^+ characteristics, as can be seen from the following form of (3+):

$$d\theta + \frac{\sin 2\mu}{2\gamma}\frac{dp}{p} = 0 \quad \text{on } C^+: \quad \frac{dy}{dx} = \tan(\theta + \mu). \tag{18}$$

Taking both $\theta = \theta(\beta)$ and $p = p(\beta)$ along with $r^- = r^-(\alpha)$ overdetermines the problem however, since any one of θ, P and r^- can be written as a function of the other two (and s). This was noted by Eggers *et al.* (1953). In their generalized shock expansion method it is resolved by averaging results assuming $r^- = r^-(\alpha)$ and $\theta = \theta(\beta)$ with those assuming $r^- = r^-(\alpha)$ and $p = p(\beta)$ (see Hayes & Probstein 1966, p. 498). Meyer (1957), on the other hand, implicitly drops the assumption $p = p(\beta)$, and uses the solution $r^- = r^-(\alpha)$ and $\theta = \theta(\beta)$, which satisfies (10) exactly, but does not satisfy (7).

In the present formulation, it appears to be more consistent to approach the problem in either of two ways: in equation (10) assume either (i) the left-hand side or (ii) the right-hand side is zero. Then solve (10) together with the remaining equation, (7).

In case (i), the solution becomes $\theta = \theta(\beta)$, $p = p(\beta)$ and $s = s(\alpha)$. The function $\theta(\beta)$ is determined by the boundary condition, and $p(\beta)$ must be determined by the shock conditions. It then happens that over the rear half of the airfoil, $\beta > \beta(1)$, $p(\beta)$ cannot be found, since no data is specified on the rear shock. This difficulty does not arise in approach (ii), which is the one we adopt.

This approach can be thought of more simply as arising from the assumption that θ is constant on C^+ characteristics, rather than the assumption that r^- is constant on streamlines. If $\theta_\alpha = 0$, then (10) reduces to

$$(\theta - P(\mu))_\beta = 0 \quad \text{or} \quad \theta - P(\mu) = -P_0(\alpha), \tag{19}$$

where $P_0(\alpha) = P[\mu(\alpha, \beta(\alpha))] - \theta(\alpha, \beta(\alpha))$. Substitution of $\theta = P(\mu) - P_0(\alpha)$ in the remaining equation, (7), then gives

$$2P(\mu)_\alpha - P_0'(\alpha) = \frac{\sin 2\mu}{2\gamma} s'(\alpha). \tag{20}$$

$P_0(\alpha)$ and $s(\alpha)$ are both given explicitly by the shock conditions, so (20) can be regarded as an ordinary differential equation for μ, in which β enters only as a parameter. It is nonlinear, but can be readily solved using standard numerical methods. The initial and final values of μ along a given C^+ characteristic are both given, by the boundary condition and the shock conditions, respectively, which allows us to solve for the free boundary $\beta(\alpha)$. The solution in the $\alpha\beta$ plane is then completed by computing $\theta(\alpha, \beta) = P(\mu(\alpha, \beta)) - P_0(\alpha)$. The solution for θ, μ and s in the $\alpha\beta$ plane is independent of x and y, because (10), the only equation in which x or y appears, is neglected. The transformation back to the xy plane is found by solving (17) for $A(\alpha)$ (also a simple numerical calculation) and evaluating the integrals (14) and (15). The solution obtained from this approximation will satisfy the boundary condition and all three shock conditions, but will satisfy (10) only approximately.

This approach requires more work (the solution of an ordinary differential equation on each C^+ characteristic) than approach (i) or the generalized shock expansion method, but has been found to be more accurate. Additional support for this choice is lent by the fact that the factor multiplying θ_α in (10) is in general quite small. Approach (i) has however been found useful for calculating the flow behind the tail shock, where method (ii) is difficult to employ (see appendix B).

5. Numerical method

Our approximate solution does not satisfy (10), or, equivalently, the C^- equation (8). In this section we present a simple iterative method for correcting the solution so that it will satisfy all the equations and conditions.

The approximate solution is computed on a rectangular grid in the $\alpha\beta$ plane (as shown in figure 3), which is then used in the numerical method. The front shock $\beta(\alpha)$ is therefore kept fixed throughout the iterations. This fixes the normalization of α, so for every iteration beyond the original approximation $\eta(\alpha)$ is not given by (12) and must be found as part of the solution. This also implies that $\alpha = 1$ no longer will correspond exactly to $x, y \to \infty$.

Given the approximate solution for θ, μ, s and x in the $\alpha\beta$ plane, a corrected value of r^- is computed from the C^- equation (3 –), or (8), starting at the shock with the

value given by the shock conditions and numerically integrating downward along the C^- characteristics:

$$r^- = r^-_{\text{shock}} - \int_{C^-} \frac{\sin 2\mu}{2\gamma}\, ds. \tag{21}$$

In particular, this determines a new value $r^-(0,\beta)$ at the airfoil, which determines a new value of $r^+(0,\beta)$ there, since $r^+ = 2\theta - r^-$, and $\theta(0,\beta)$ is given by the boundary condition. With this as an initial value, a new r^+ is computed everywhere by numerically integrating (3+), or (7), along C^+ characteristics:

$$r^+(\alpha,\beta) = r^+(0,\beta) + \int_0^\alpha \frac{\sin 2\mu}{2\gamma}\, s'(\alpha)\, d\alpha. \tag{22}$$

With r^+ and r^- thus determined, the solution given by

$$\theta = \tfrac{1}{2}(r^+ + r^-), \quad \mu = P^{-1}[\tfrac{1}{2}(r^+ - r^-)],$$

and s will satisfy the differential equations and the boundary condition. However, the new value of $r^+(\alpha,\beta(\alpha))$ will not in general satisfy the shock conditions, and hence will imply a different value for the shock angle $\eta(\alpha)$. This can be used to determine a new initial value $r^-(\alpha,\beta(\alpha))$ for integrating (21), and the procedure can be repeated.

The transformation back to the xy plane is found by numerically solving the integral equation (17) and evaluating the integrals (14) and (15). This must be done at each iteration, since x and y enter into the computation of the integral in (21). The C^- characteristics are oblique to the (α,β) co-ordinate system, so at each point a small section of the C^- characteristic through that point is extended backwards to intersect a grid line, and a one-step integration is used to compute r^-. We might, in place of equation (8), have integrated (10), which has the advantage that r^- is differentiated only with respect to β, so that the integration would be along the co-ordinate lines, as in (22). In practice, however, this has been found unadvantageous. The solution does not converge as quickly, and may not converge at all without modification (see Chong & Sirovich 1980). We attribute this to the fact that small variations in r^- are naturally propagated along the C^- characteristics.

This scheme has been implemented using second-order numerical methods (trapezoidal rule, improved Euler method, etc.). Some results are given in the next section.

6. Results

Calculations have been performed for several airfoils over a range of Mach numbers. The results presented in figures 1 and 3–7 are for a symmetric circular arc airfoil with thickness ratio 0·25 at upstream Mach number $M_0 = 4$. In figures 8–10 results from the additional cases $M_0 = 2{\cdot}5$ and 7·5, for the same airfoil, are included as well. These cases were chosen in part for the interesting effects they exhibit.

The iteration scheme converges quite rapidly, based on a comparison of the solutions at successive iterations. In table 1, the maxima (over all grid points) of the differences in the values of θ, μ and x are given for the case $M_0 = 7{\cdot}5$ (the most slowly convergent of the three cases). The greatest differences are in x and usually occur near $\alpha = 1$, where $x \to \infty$. The errors in x are smaller closer to the airfoil. For thinner airfoils or lower Mach numbers, fewer iterations are required for the same accuracy. In the case

Iteration	$\Delta\theta/\theta(0, 0)$	$\Delta\mu/\mu$	$\Delta x/x$
1	0·0595	0·1170	0·3701
2	0·0141	0·0096	0·1221
3	0·0008	0·0007	0·0112
4	0·0002	0·0006	0·0017
5	0·0001	0·0003	0·0009

TABLE 1

of a 10 % thick parabolic arc airfoil, for example, even at $M_0 = 10$ the difference between the approximate and exact solutions is less than one per cent in θ and μ and six per cent in x. In such a case there is little reason to go beyond the approximate solution.

The case $M_0 = 2{\cdot}5$ is discussed in Holt (1977). Figure 4 contains a comparison of the leading shock when computed by our approximate and exact methods, the BVLR method (an exact numerical method), and generalized shock expansion theory (the latter and the BVLR solution are taken from Holt 1977, p. 77). In this case, our approximate solution is indistinguishable from the exact solution. The small difference between these and the BVLR solution is probably attributable to copying errors.

Figure 5 contains plots of pressure contours in the xy plane and the value of $\log p$ on the airfoil surface and on the line of symmetry behind the airfoil. Comparison with figure 1 shows that the contour lines between the lead and tail shocks are nearly identical to C^+ characteristics, i.e. the pressure is approximately constant on C^+ characteristics. This was seen in § 4 to be related to the fact that θ is approximately constant on C^+ characteristics, which in turn is related to the fact that r^- is approximately constant on streamlines. The latter two assumptions are illustrated in figures 6 and 7.

In figure 6, the deflection angle θ is plotted versus α on each of the C^+ characteristics shown in figure 3. In the region behind the tail shock θ is very nearly zero ($|\theta| < 0{\cdot}005$) everywhere. The variation in θ along each characteristic is quite small, with the most serious departure occurring on the characteristics originating from the rear part of the airfoil. These characteristics tend to intersect the tail shock fairly close to the airfoil, however. A related phenomenon is that the principal characteristics are nearly straight. This however does not remain true in the region behind the airfoil.

Figure 7 shows the variation of r^- with β on each streamline of figure 3. Somewhat remarkably the assumption $r^- = -P_0(\alpha)$ is better at the airfoil than a short distance away. The assumption is less satisfactory behind the tail shock. The rapid downstroke of the r^- curves also indicates a large value of θ_α, although θ itself remains quite small.

The entropy jumps created by the lead and tail shocks are given in figure 8 for the three cases $M_0 = 2{\cdot}5$, 4·0 and 7·5. The entropy variation along the tail shock has a two-scale appearance, especially at the higher Mach numbers, which shows a very rapid decrease in strength in the initial portion of the shock. The slower variation in entropy follows that induced by the front shock. Looking at figure 1, we see that the streamlines spread apart rapidly as the flow passes the midchord position. The inclination of the flow incident upon the tail shock therefore decreases rapidly, which causes a correspondingly rapid decrease in shock strength.

Another important effect is also at work in this region. The gas, which is compressed

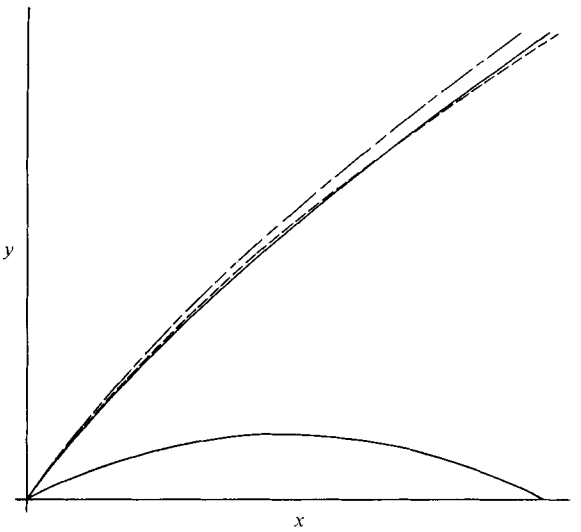

FIGURE 4. Front shock for flow field of figure 1 as computed by: present approximate and exact methods (——), BVLR method (- - -), generalized shock expansion method (— - —).

at the front shock, in following the profile past the midchord experiences a rapid expansion, which is strong enough that the local Mach number at the trailing edge exceeds the upstream value ($M = 9{\cdot}83$ for the $M_0 = 7{\cdot}5$ case). This recovery process is largely cut off by the tail shock, however, since the large negative value of θ on the after part of the airfoil causes the principal characteristics to have negative slopes, so that waves originating there must intersect the tail shock near the airfoil. As a result the Mach number along the tail shock falls off rapidly, which augments the rapid decrease in strength of the tail shock. For the case $M_0 = 7{\cdot}5$ the Mach number along the shock even falls below 7·5.

The pressure field behind the airfoil (figure 5) also contains interesting features. In spite of the very high shock strength at the trailing edge, the pressure jump through the shock does not quite bring p up to the equilibrium pressure $p = 1$. There is a rapid pressure increase immediately behind the trailing edge, in which p increases above the equilibrium value, reaching a maximum about one chord length out. The return to equilibrium from this point is very gradual. The total variation in pressure behind the tail shock is quite small compared with that along the airfoil surfaces.

Far behind the airfoil $p \to 1$ and $\theta \to 0$. It then follows from the equation of state that

$$a^2 = \exp[-(\gamma - 1)\, s_3(\alpha)/\gamma],$$

where $s_3(\alpha)$ is given by figure 8. From (1), we can then compute the velocity q at infinity. This is shown in figure 9 for $M_0 = 2{\cdot}5$, 4·0 and 7·5. As a result of the non-uniform entropy, the flow at infinity has a vorticity distribution.

A feature which is difficult to perceive from figure 1 or figure 5 is that the tail shock angle is not monotonic. In figure 10 the variation of the slope of the tail shock is given for the three cases we have discussed. In each case the shock angle decreases on leaving the trailing edge. (This result has been verified independently by J. C. Townsend 1979 (private communication), using a numerical method developed by

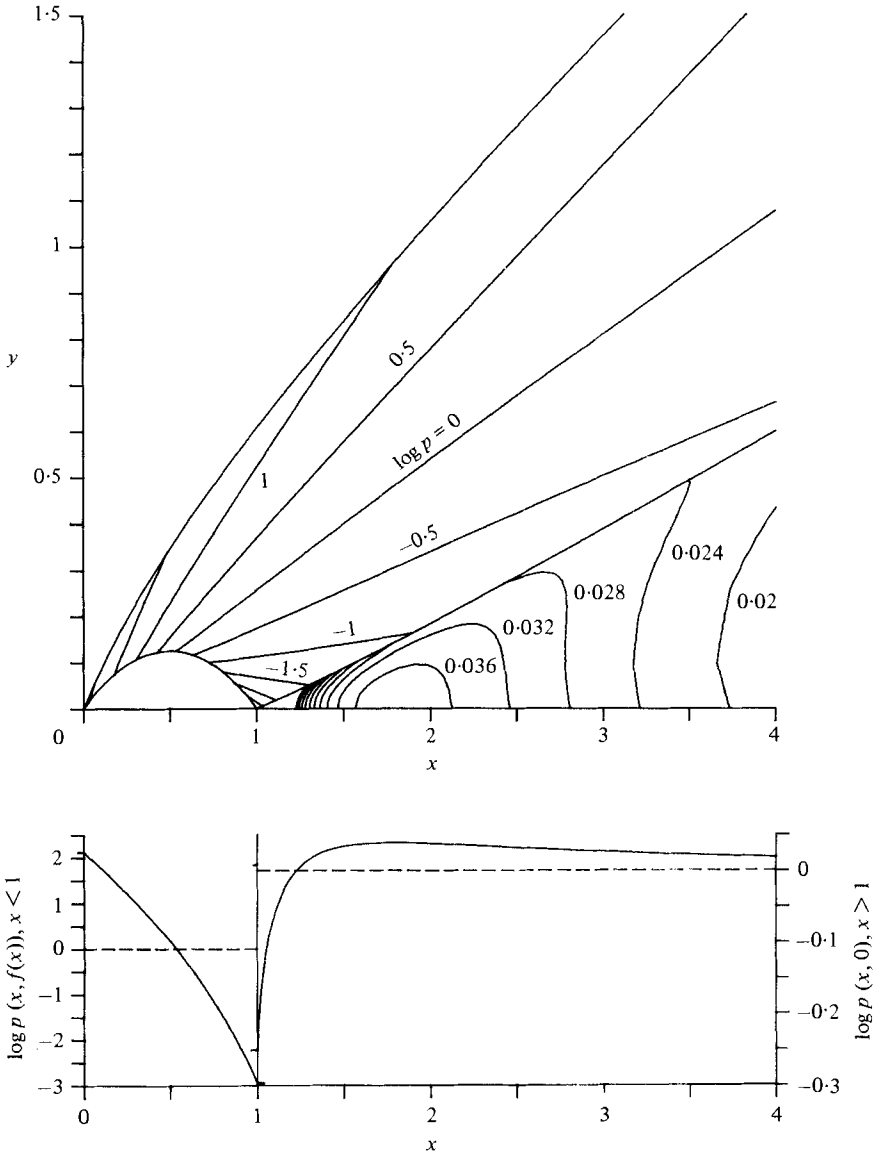

FIGURE 5. Upper graph: pressure contours in flow field of figure 1. Lower graph: $\log p$ *vs.* x at $\alpha = 0$. Note different scales for $0 < x < 1$ and $x > 1$.

M. D. Salas.) This is contrary to what is observed for lower Mach numbers or thinner bodies. We have seen that the inclination of the incident flow decreases along the shock. If the Mach number upstream of the shock were constant, this would predict a decrease in shock angle. The Mach number actually decreases along the shock however, which tends to increase the shock angle. At high Mach numbers the shock angle is more dependent on the flow angle than on the Mach number, as can be seen from the fact that the shock polars for different Mach numbers approach a limiting curve as $M \to \infty$ (see e.g. Liepmann & Roshko 1957, p. 87). In these cases, near the trailing edge the decreasing flow angle dominates. Farther away from the airfoil, or

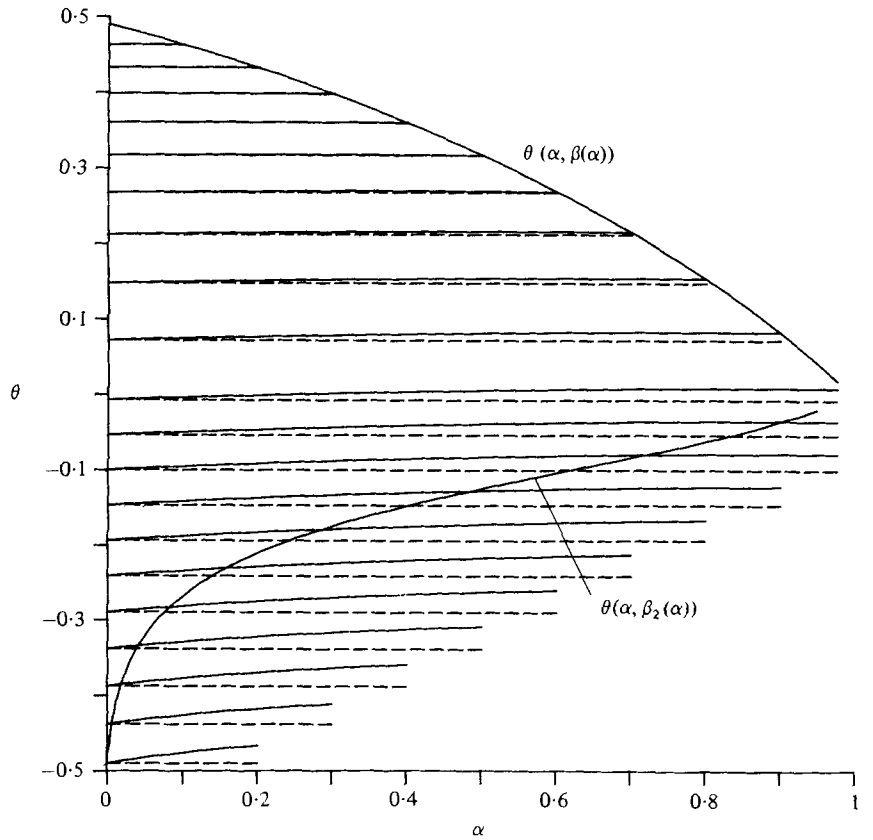

FIGURE 6. Flow angle θ *vs.* α on each C^+ characteristic of figure 3. Dashed lines are constant values $\theta = \tan^{-1} f'(\beta)$ for comparison. Values along front shock $\beta(\alpha)$ and tail shock $\beta_2(\alpha)$ are also given.

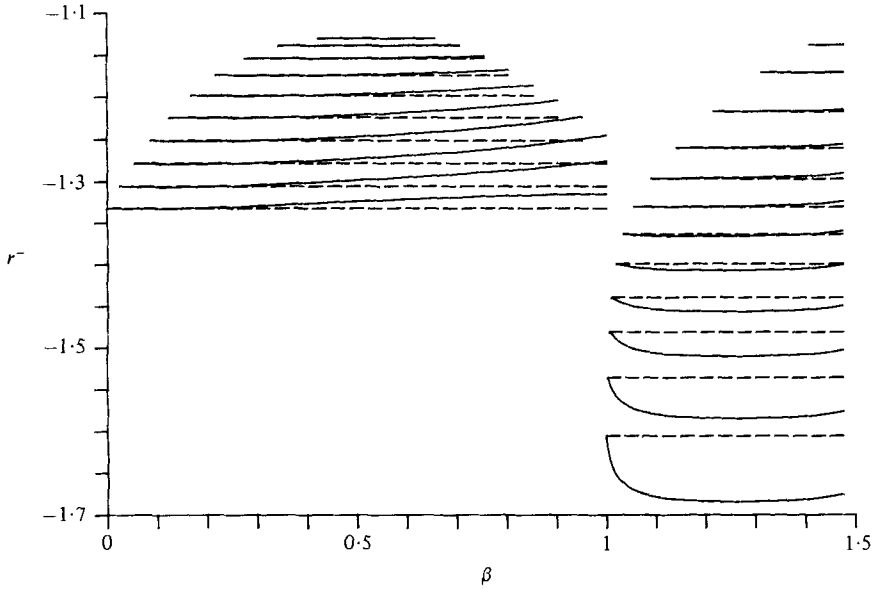

FIGURE 7. Riemann invariant r^- *vs.* β on each streamline of figure 3. Dashed lines are constant values $r = -P_0(\alpha)$ for comparison.

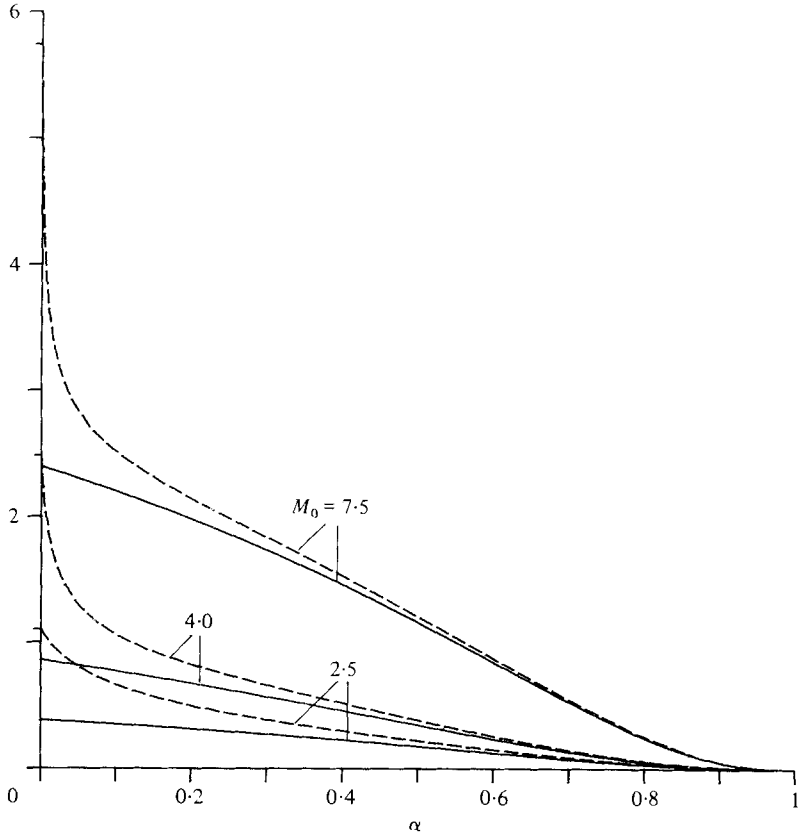

FIGURE 8. Entropy $s(\alpha)$ (——) in region between front and tail shocks, and $s_3(\alpha)$ (– – –) in region behind tail shock, for 25% circular arc airfoil at upstream Mach numbers $M_0 = 2·5$, 4·0, and 7·5.

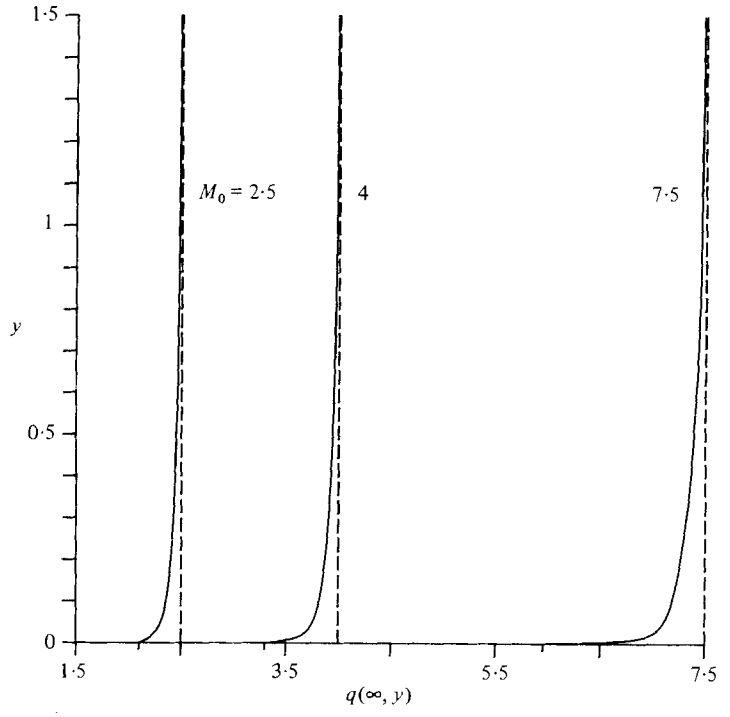

FIGURE 9. Velocity profiles far behind airfoil for $M_0 = 2·5$, 4·0 and 7·5. Dashed lines are asymptotic values, M_0.

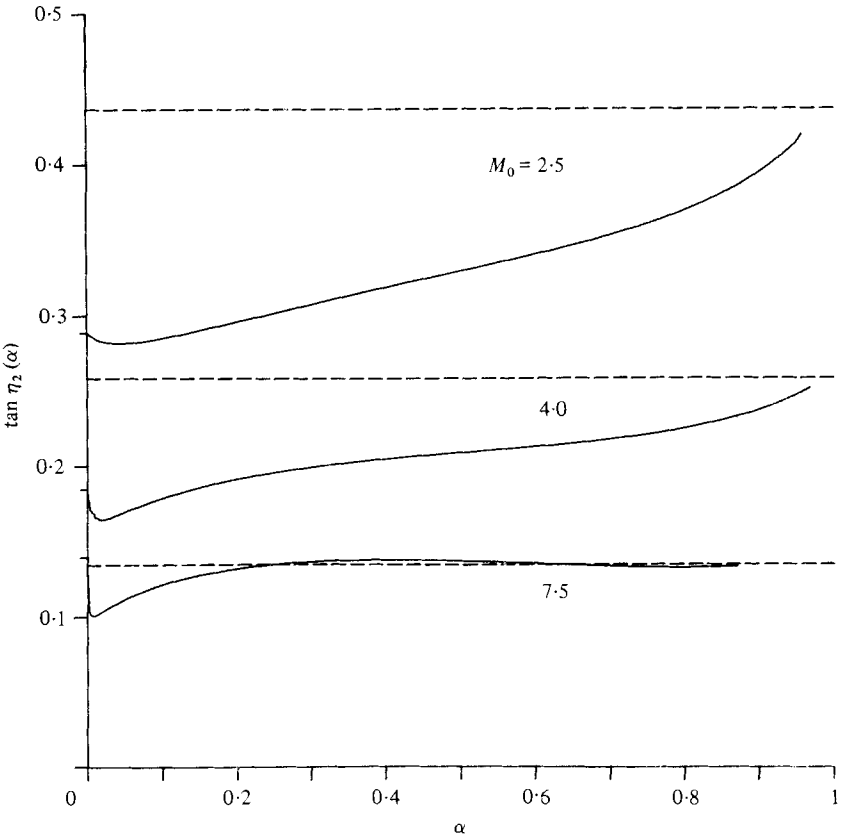

FIGURE 10. Tail shock slope tan $\eta_2(\alpha)$ for $M_0 = 2{\cdot}5$, 4·0 and 7·5. Dashed lines are asymptotic values, tan μ_0.

in problems with lower Mach numbers or thinner airfoils, the effect of decreasing Mach number dominates.

In the case $M_0 = 7{\cdot}5$ the shock angle undergoes a second oscillation in which it rises above the Mach angle at infinity, μ_0. This is explained by the rapid fall-off of Mach number along the shock, below its value at infinity. A final item of note in figure 10 is that for $M_0 = 7{\cdot}5$ the shock angle actually starts off with a value which is greater than μ_0. As $M_0 \to \infty$ the upstream Mach angle μ_0 goes to zero, as does the Mach angle at the trailing edge, since the Mach number there also increases. The shock slope at the trailing edge approaches a finite value however, which depends on the airfoil slope at the trailing edge.

7. Conclusions

The methods we have presented are useful in computing two-dimensional flow fields about airfoils. The approximate solution is accurate enough for many cases of interest, and the numerical method furnishes a rapid correction to the solution in those cases where it is not. The characteristic-streamline co-ordinate system is useful both for the computation of the approximate solution and the corrections, and is also convenient for displaying and interpreting the results.

The use of the streamlines as one co-ordinate and the iterative nature of the numerical calculation make the method convenient for the incorporation of a boundary-layer correction. In a boundary thickness method, for example, a succession of inviscid calculations are performed with a changing airfoil shape. The changing shape could be easily included in the present iteration method.

In response to a referee's request for comparison with other integration schemes, we asked Dr James C. Townsend of the NASA Langley Research Center to run some speed trials on their CDC Cyber 175 computer comparing our code with a 'marching' method developed there. At the lowest Mach number, $M_0 = 1{\cdot}25$, our scheme runs about seven times faster than the marching method, while at the highest Mach number, $M_0 = 10$, our scheme was slightly slower. The present method is most efficient at low Mach numbers where the approximate solution is most accurate and the fewest iterations are required. This is in contrast to the marching method, where low Mach number necessitates a short step size for stability, and hence longer computation times. While these trials give some idea of relative speed they cannot be considered definitive.

This work was supported by the National Aeronautics and Space Administration under NASA Grant no. NSG 1617. The authors would like to thank Dr James C. Townsend for carrying out a number of computations which were very useful in the course of this research.

Appendix A. Case of an arbitrary gas

For an arbitrary gas, the equations of motion in characteristic form can be written (Hayes & Probstein 1966, p. 484)

$$ds = 0 \quad \text{on} \quad dy/dx = \tan\theta, \tag{A 1}$$

$$d\theta \pm \Phi dp = 0 \quad \text{on} \quad dy/dx = \tan(\theta \pm \mu), \tag{A 2}$$

where $\Phi = p_0/(\rho_0 a_0^2 \rho q^2 \tan\mu)$. We can consider Φ to be a function of p and s. By introducing the variables

$$\omega(p,s) = \int \Phi(p,s)\,dp \quad \text{and} \quad \Omega(p,s) = \partial\omega(p,s)/\partial s,$$

which are defined so that $d\omega = \Phi dp + \Omega ds$, (A 2) can be written as

$$d\theta \pm d\omega = \pm \Omega ds \quad \text{on} \quad dy/dx = \tan(\theta \pm \mu). \tag{A 3}$$

If ω and Ω are now regarded as functions of μ and s, (A 1) and (A 3) are three equations in three unknowns: θ, μ and s. Equations (3) are a special case of (A 3) in which $\omega = P(\mu)$ and $\Omega = (\sin 2\mu)/2\gamma$.

The transformation to $\alpha\beta$ co-ordinates goes through for the most part as before. Equations (6)–(8) in the general case become

$$s_\beta = 0, \quad (\theta+\omega)_\alpha = \Omega s'(\alpha),$$

$$\left(\frac{\partial}{\partial\alpha} + w\frac{\partial}{\partial\beta}\right)(\theta-\omega) = -\Omega s'(\alpha),$$

where w is still given by (9). The counterpart of (13) is

$$0 = \frac{x_{\alpha\beta}}{x_\alpha} + (\mu+\omega)_\beta \cot\mu + (\theta+\mu)_\beta \tan(\theta+\mu).$$

This equation can in principle be solved in the same manner as (13), but, depending on the form of ω, we may not have an explicit integral like (14).

The assumption $\theta_\alpha = 0$ in the general case implies $(\theta - \omega)_\beta = 0$ or $\theta - \omega = -\omega_0(\alpha)$. The resulting approximation can be expected to be valid at least in cases in which the behaviour of the gas does not differ too greatly from that of a perfect gas with constant specific heats and $\gamma = 1{\cdot}4$. In particular, it has been shown (see Hayes & Probstein 1966, § 7.2) that shock expansion theory tends to lose accuracy if γ is allowed to approach 1.

Appendix B. Tail shock for a symmetric airfoil

In general, the solutions above and below the airfoil can be computed independently, up to the appearance of the tail shocks. The flows from the top and bottom interact behind the airfoil, which complicates the computation of the tail shocks and the flow behind them. The upper and lower regions behind the airfoil are separated by a contact discontinuity, or slipstream, across which θ and p are continuous, but the other variables jump. In the case of an airfoil symmetric with respect to the x axis the slipstream coincides with the x axis, and can be considered a rigid boundary. The problem is still quite different from the front shock problem, because the flow upstream of the tail shock is not uniform.

The transformation to $\alpha\beta$ co-ordinates behind the tail shock can be chosen differently than that ahead of it. In particular, it is more proper to regard the C^- characteristics as the principal characteristics, since the C^+ waves are only produced as reflections of the C^- waves, which originate at the tail shock. The approximate solution is somewhat more accurate if the C^- characteristics are used. On the other hand, for numerical work it is better to take the C^+ characteristics as the β co-ordinates, because this has the effect of putting more points near the trailing edge, where a rapid variation in the solution occurs. We keep α constant on streamlines as they cross the shock, and normalize β behind the tail shock so that the infinite region behind the tail shock is mapped into a finite region in the $\alpha\beta$ plane. In the calculations presented here, this was done by setting $\beta_3(\alpha) = 1 + \frac{1}{2}\alpha$, producing the triangular region shown in figure 3.

The approximate solution used for the flow over the airfoil cannot be conveniently employed for the flow behind the tail shock, because the non-uniform flow to its left makes it impossible to calculate $P_0(\alpha)$ and $s(\alpha)$ *a priori* for use in (20). Therefore the simpler of the approximations given in § 4 is used: $\theta = \theta_3(\beta)$, $p = p_3(\beta)$, and $s = s_3(\alpha)$. All the characteristics intersect the x axis, where $\theta = 0$, so $\theta_3(\beta) = 0$, and hence in this approximation $\theta = 0$ everywhere. This turns out to be quite accurate (see § 6). Given that $\theta = 0$ behind the tail shock, it is possible to solve the shock conditions for the tail shock angle $\eta_2(\alpha)$, in terms of the solution upstream of the tail shock, which we assume has been previously computed. This also determines $p_3(\beta)$ and $s_3(\alpha)$, and gives an ordinary differential equation to solve for the tail shock $\beta_2(\alpha)$. It is possible to derive expressions for x and y similar to (14) and (15) for the region behind the tail shock, which will involve a new function $A_3(\alpha)$. An explicit solution for $A_3(\alpha)$ can be found in this case, involving the computed tail shock trajectory.

The iteration scheme proceeds essentially as before. Given $r^-(\alpha, \beta_3(\alpha))$ from the shock conditions, we integrate (21) along C^- characteristics down to the slipstream

$\alpha = 0$. Then we reset $r^+(0,\beta) = -r^-(0,\beta)$, and integrate (22) upwards to $\beta_3(\alpha)$. The new r^+ and r^- define a new $\theta(\alpha,\beta_3(\alpha))$, which is used to solve for a new shock $\beta_3(\alpha)$ and new functions $\eta_2(\alpha)$, $s_3(\alpha)$, and $r^-(\alpha,\beta_3(\alpha))$, with which we start the next iteration.

REFERENCES

Adamson, T. C. 1968 *J. Fluid Mech.* **34**, 735.

Babenko, K. I., Voskresenskiy, G. P., Lyubimov, A. N. & Rusanov, V. V. 1966 Three-dimensional flow of ideal gas past smooth bodies. *N.A.S.A. Tech. Transl.* F-380.

Caughey, D. A. 1969 Second-order wave structure in supersonic flows. *N.A.S.A.* CR-1438.

Chong, T. H. & Sirovich, L. 1980 *Phys. Fluids* **23**, 1296.

Eggers, A. J., Syvertson, C. A. & Kraus, S. 1953 *N.A.C.A. Rep.* no. 1123.

Epstein, P. S. 1931 *Proc. Nat. Acad. Sci.* **17**, 532.

Friedrichs, K. O. 1948 *Comm. Pure Appl. Math.* **1**, 211.

Hayes, W. D. & Probstein, R. F. 1966 *Hypersonic Flow Theory*, vol. I. Academic.

Holt, M. 1977 *Numerical Methods in Fluid Dynamics*. Springer.

Jones, J. G. 1963 *J. Fluid Mech.* **17**, 506.

Liepmann, H. W. & Roshko, A. 1957 *Elements of Gasdynamics*. Wiley.

Lighthill, M. J. 1960 *Higher Approximations in Aerodynamic Theory*. Princeton University Press.

Mahony, J. J. 1955 *J. Aero. Sci.* **22**, 673.

Mahony, J. J. & Skeat, P. R. 1955 *Austr. Aero. Res. Lab., Aero. Note* 147.

Meyer, R. E. 1957 *Q. Appl. Math.* **14**, 433.

Meyer, R. E. 1960 Theory of characteristics in inviscid gas dynamics, *Handbuch der Physik*, vol. IX. Springer.

Salas, M. D. 1976 *A.I.A.A. J.* **14**, 583.

Sirovich, L. & Chong, T. H. 1980 *Phys. Fluids* **23**, 1291.

Taylor, T. D., Ndefo, E. & Masson, B. S. 1972 *J. Comp. Phys.* **9**, 99.